

Dynamic Modeling of Linear Object Deformation based on Differential Geometry Coordinates

Hidefumi Wakamatsu

Dept. Manufacturing Science, Osaka Univ.
Suita, Osaka 565-0871, Japan
wakamatu@mapse.eng.osaka-u.ac.jp

Kousaku Takahashi and Shinichi Hirai

Dept. Robotics, Ritsumeikan Univ.
Kusatsu, Shiga 525-8577, Japan
hirai@se.ritsumei.ac.jp

Abstract—This paper describes the dynamic modeling of linear object deformation based on differential geometry coordinates. Deformable linear objects such as cables and strings are widely used in our daily life, electric industries, medical operations. Modeling, control, and manipulation of deformable linear objects are keys to many applications. We have proposed the differential geometry coordinates to describe the 2D/3D deformation of a linear object with the minimum number of parameters. Based on this description, we have formulated the static deformation of a linear object using the differential geometry coordinates but the dynamic deformation has not been investigated yet.

In this paper, we apply differential geometry coordinates to the dynamic modeling of linear objects. First, we formulate the dynamic 2D deformation of an inextensible linear object based on a differential geometry coordinate system. Second, we show simulation results using the proposed modeling technique. Next, we apply the proposed dynamic modeling to the control of a flexible link.

Index Terms—deformation, linear object, dynamics, modeling, simulation, control

I. INTRODUCTION

Deformable linear objects such as cables and strings are widely used in our daily life, electric industries, and medical operations. Modeling, control, and manipulation of deformable linear objects are keys to many applications: robotic systems capable of manipulating linear objects, automatic handling of electric cables and wires, and simulation of medical surgery with threads.

Deformed shape of threads in a fabric has been described geometrically [1]. In computer graphics, the particle-based approach has been applied to simulate the motion of hairs. Flexure and extension of hairs have been described in [2], while flexure and torsion of hairs have been described in [3], implying that flexure, torsion, and extension of a linear object can be described using particle-based approach. Deformation of a linear object can be modeled using beam elements in FEM. Spline-based modeling has been applied to the realtime simulation of soft tissues as well as sutures in surgery [4]. Linear objects have been approximated using beams in the engineering community; models exist to describe small deflection of beams [5], and also large deformation using nonlinear beam finite elements[6]. Fast algorithms have been introduced to describe linear object deformation using the Cosserat formulation [7].

We have proposed the *differential geometry coordinates* to describe the 2D/3D deformation of a linear object

with the minimum number of parameters [8]. We have established static formulation of a deformable linear object using the differential geometry coordinates but the dynamic modeling has not been investigated yet. In this paper, we apply differential geometry coordinates to the dynamic modeling of linear objects. First, we formulate the dynamic 2D deformation of an inextensible linear object based on a differential geometry coordinate system. Second, we show simulation results using the proposed modeling technique. Next, we apply the proposed dynamic modeling to the control of a flexible link.

II. DYNAMIC MODELING OF LINEAR OBJECT DEFORMATION

In this section, we formulate the 2D deformation of an inextensible linear object. Assume that a linear object of length L bends in frame $O - xy$, as illustrated in Figure 1. One end of the object is fixed to but can rotate around the origin. An external torque τ is applied around this end. The other end is free to move. Let s be the distance from the fixed end along the linear object. Let $P(s)$ be a point on the object specified by distance s . Let $\theta(s, t)$ be the angle from the horizon at point $P(s)$ and time t . Position of point $P(s)$ at time t is then described by

$$\begin{bmatrix} x(s, t) \\ y(s, t) \end{bmatrix} = \int_0^s \begin{bmatrix} \cos \theta(u, t) \\ \sin \theta(u, t) \end{bmatrix} du.$$

Differentiating the above equation with respect to time t yields the velocity vector at point $P(s)$ given by

$$\begin{bmatrix} \dot{x} \\ \dot{y} \end{bmatrix} = \int_0^s \begin{bmatrix} -\sin \theta \\ \cos \theta \end{bmatrix} \dot{\theta} du.$$

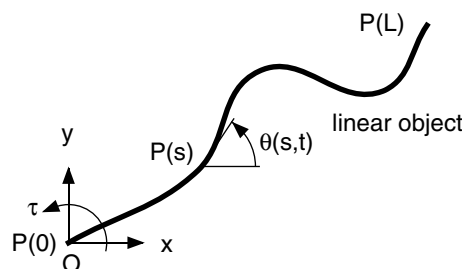


Fig. 1. Dynamic 2D deformation of inextensible linear object

Lagrangean formulation requires the kinetic energy of the object. Kinetic energy T can be described as follows:

$$T = \int_0^L \frac{1}{2} \rho (\dot{x}^2 + \dot{y}^2) ds.$$

where ρ denotes the line density at point $P(s)$, which may depend on s .

Let us divide region $[0, L]$ into n small regions with a constant interval $h = L/n$. Let P_0 through P_n be nodal points on the region, of which coordinates are denoted as s_0 through s_n . Applying piecewise linear approximation to function $\theta(s, t)$, the function can be described by

$$\theta(s, t) = \theta_i(t)N_{i,j}(s) + \theta_j(t)N_{j,i}(s) \quad (1)$$

in a divided region $[s_i, s_j]$, where $\theta_i(t) = \theta(s_i, t)$ and $\theta_j(t) = \theta(s_j, t)$. Shape function $N_{i,j}(s)$ takes 1 at s_i and 0 at s_j while $N_{j,i}(s)$ takes 0 at s_i and 1 at s_j . Let A_i be a set of nodal points adjacent to nodal point P_i :

$$A_i = \{j \mid \text{nodal point } P_j \text{ is adjacent to nodal point } P_i\}.$$

Finite element approximation is applied to the kinetic energy T of a deformable linear object. First, let us introduce the following integrals:

$$S_{i,j}(s; \theta_0, \dots, \theta_n) = \int_0^s \{\sin \theta(u, t)\} N_{i,j}(u) du,$$

$$C_{i,j}(s; \theta_0, \dots, \theta_n) = \int_0^s \{\cos \theta(u, t)\} N_{i,j}(u) du.$$

These integrals $S_{i,j}$ and $C_{i,j}$ depend on θ_0 through θ_n . The velocity components at point $P(s)$ are given by

$$\dot{x}(s, t) = \sum_{[s_i, s_j]} \left\{ -\dot{\theta}_i(t)S_{i,j}(s) - \dot{\theta}_j(t)S_{j,i}(s) \right\},$$

$$\dot{y}(s, t) = \sum_{[s_i, s_j]} \left\{ \dot{\theta}_i(t)C_{i,j}(s) + \dot{\theta}_j(t)C_{j,i}(s) \right\}.$$

The square of each velocity component is then described by

$$\dot{x}^2 = \sum_{[s_i, s_j]} \sum_{[s_k, s_l]} \left\{ \dot{\theta}_i \dot{\theta}_k S_{i,j} S_{k,l} + \dot{\theta}_i \dot{\theta}_l S_{i,j} S_{l,k} + \dot{\theta}_j \dot{\theta}_k S_{j,i} S_{k,l} + \dot{\theta}_j \dot{\theta}_l S_{j,i} S_{l,k} \right\},$$

$$\dot{y}^2 = \sum_{[s_i, s_j]} \sum_{[s_k, s_l]} \left\{ \dot{\theta}_i \dot{\theta}_k C_{i,j} C_{k,l} + \dot{\theta}_i \dot{\theta}_l C_{i,j} C_{l,k} + \dot{\theta}_j \dot{\theta}_k C_{j,i} C_{k,l} + \dot{\theta}_j \dot{\theta}_l C_{j,i} C_{l,k} \right\}.$$

Thus, kinetic energy T is described by a quadratic form with respect to $\dot{\theta}_0$ through $\dot{\theta}_n$ given by

$$T = \frac{1}{2} \sum_i \sum_k m_{i,k} \dot{\theta}_i \dot{\theta}_k \quad (2)$$

where

$$m_{i,k} = \int_0^L \sum_{j \in A_i} \sum_{l \in A_k} \rho (S_{i,j} S_{k,l} + C_{i,j} C_{k,l}) ds. \quad (3)$$

Let M be a matrix of which the (i, k) -th element is given by $m_{i,k}$. Matrix M is referred to as the *inertial matrix*, which is symmetric and positive-definite.

Let us compute partial derivative of inertia matrix component $m_{i,k}$ with respect to a generalized coordinate θ_r . Differentiating eq.(1) with respect to a generalized coordinate θ_r , we have

$$\frac{\partial}{\partial \theta_r} \theta(s, t) = \sum_{p \in A_r} N_{r,p}.$$

This is followed by

$$\frac{\partial S_{i,j}}{\partial \theta_r} = \int_0^s \{\cos \theta(u, t)\} \left\{ \sum_{p \in A_r} N_{r,p} \right\} N_{i,j} du,$$

$$\frac{\partial C_{i,j}}{\partial \theta_r} = \int_0^s \{-\sin \theta(u, t)\} \left\{ \sum_{p \in A_r} N_{r,p} \right\} N_{i,j} du.$$

Thus,

$$\frac{\partial S_{i,j}}{\partial \theta_r} = \begin{cases} \int_0^s \{\cos \theta\} (N_{i,j})^2 du & r = i \\ \int_0^s \{\cos \theta\} N_{i,j} N_{j,i} du & r = j \\ 0 & \text{otherwise} \end{cases},$$

$$\frac{\partial C_{i,j}}{\partial \theta_r} = \begin{cases} \int_0^s \{-\sin \theta\} (N_{i,j})^2 du & r = i \\ \int_0^s \{-\sin \theta\} N_{i,j} N_{j,i} du & r = j \\ 0 & \text{otherwise} \end{cases}.$$

Consequently, partial derivative $\partial m_{i,k} / \partial \theta_r$ is given by

$$\frac{\partial m_{i,k}}{\partial \theta_r} = \int_0^L \sum_{j \in A_i} \sum_{l \in A_k} \rho \left(\frac{\partial S_{i,j}}{\partial \theta_r} S_{k,l} + S_{i,j} \frac{\partial S_{k,l}}{\partial \theta_r} + \frac{\partial C_{i,j}}{\partial \theta_r} C_{k,l} + C_{i,j} \frac{\partial C_{k,l}}{\partial \theta_r} \right) ds. \quad (4)$$

Lagrange equation of motion with respect to a generalized coordinate θ_i is formulated as follows:

$$\frac{\partial L}{\partial \theta_i} - \frac{d}{dt} \frac{\partial L}{\partial \dot{\theta}_i} = 0.$$

Contribution of kinetic energy T to the above Lagrange equation of motion is described by

$$\sum_k S_{i,k} \dot{\theta}_k - \sum_k m_{i,k} \ddot{\theta}_k + \sum_j Y_{i,j} \dot{\theta}_j$$

where

$$S_{i,k} = \frac{1}{2} \left\{ \sum_j \left(\frac{\partial m_{k,j}}{\partial \theta_i} - \frac{\partial m_{i,j}}{\partial \theta_k} \right) \dot{\theta}_j \right\},$$

$$Y_{i,j} = \frac{1}{2} \left\{ - \sum_k \frac{\partial m_{i,j}}{\partial \theta_k} \dot{\theta}_k \right\}.$$

Since $S_{i,k} + S_{k,i}$ vanishes, matrix S of which the (i,k) -th element is given by $S_{i,k}$ is skew-symmetric. Since $Y_{i,j}$ coincides to $Y_{j,i}$, matrix Y of which the (i,j) -th element is given by $Y_{i,j}$ is symmetric. Let θ_N be a vector consisting of θ_0 through θ_n . Contribution of kinetic energy T to a set of Lagrange equations of motion with respect to θ_0 through θ_n is then summarized in a vector form as follows:

$$S\dot{\theta}_N - M\ddot{\theta}_N + Y\dot{\theta}_N. \quad (5)$$

Assume that the potential energy of the object U consists of flexural potential energy U_{flex} and gravitational potential energy U_{grav} , say,

$$U = U_{\text{flex}} + U_{\text{grav}}.$$

Assuming that the bending moment at point $P(s)$ on the object is proportional to the curvature at that point, the flexural potential energy is formulated as

$$U_{\text{flex}} = \int_0^L \frac{1}{2} R_{\text{flex}} \left(\frac{d\theta}{ds} \right)^2 ds, \quad (6)$$

where R_{flex} denotes the flexural rigidity at point $P(s)$. Assuming that rigidity R_{flex} is constant, flexural potential energy is approximated as follows:

$$U_{\text{flex}} = \sum_{[s_i, s_j]} \frac{1}{2} \begin{bmatrix} \theta_i & \theta_j \end{bmatrix}^T \frac{R_{\text{flex}}}{h} \begin{bmatrix} 1 & -1 \\ -1 & 1 \end{bmatrix} \begin{bmatrix} \theta_i \\ \theta_j \end{bmatrix}.$$

Namely, flexural potential energy is described by a quadratic form as follows:

$$U_{\text{flex}} = \frac{1}{2} \theta_N^T K \theta_N,$$

where K denotes the stiffness matrix of flexural deformation. Consequently, contribution of flexural potential energy to a set of Lagrange equations of motion is given by $-K\theta_N$. Let D be the weight per unit length at point $P(s)$. The gravitational potential energy is then given by

$$U_{\text{grav}} = \int_0^L D y(s, t) ds.$$

Let $-\mathbf{G}(\theta_N)$ be the contribution of gravitational potential energy to a set of Lagrange equations of motion. The i -th component of vector \mathbf{G} coincides with the partial derivative of U_{grav} with respect to θ_i :

$$G_i = \frac{\partial U_{\text{grav}}}{\partial \theta_i} = \int_0^L D \frac{\partial y}{\partial \theta_i} ds$$

where

$$\frac{\partial y}{\partial \theta_i} = \int_0^s \cos \theta(u, t) \left\{ \sum_{j \in A_i} N_{i,j}(u) \right\} du.$$

Applying any numerical integration, we can compute the contribution of gravitational potential energy to a set of Lagrange equations of motion. As a result, contribution of potential energy U to a set of Lagrange equations of motion

with respect to θ_0 through θ_n is summarized in a vector form as follows:

$$-K\theta_N - \mathbf{G}(\theta_N). \quad (7)$$

Lagrangian of the linear object is formulated as

$$L = T - U + \tau \theta(0, t).$$

A set of Lagrange equations of motion with respect to θ_0 through θ_n is then described as

$$S\dot{\theta}_N - M\ddot{\theta}_N + Y\dot{\theta}_N - K\theta_N - \mathbf{G}(\theta_N) + \tau = 0$$

where $\tau = [\tau, 0, \dots, 0]^T$. Let ω_N be a vector consisting of angular velocities $\dot{\theta}_0$ through $\dot{\theta}_n$. The above set of equations can be rewritten as follows:

$$\begin{aligned} \dot{\theta}_N &= \omega_N, \\ M\dot{\omega}_N &= S\omega_N + Y\omega_N - K\theta_N - \mathbf{G}(\theta_N) + \tau. \end{aligned} \quad (8)$$

Note that matrices M , S , and Y depend on vector θ_N . Individual elements of matrix M can be computed by eq.(3). Individual elements of matrices S and Y can be calculated through partial derivatives given in eq.(4). We can compute these partial derivatives using any numerical integration method.

In this section, we have formulated the 2D dynamic deformation of an inextensible linear object, which is described by one function $\theta(s, t)$. This formulation can be extended to the 2D dynamic deformation of an extensible linear object, which is described by two independent functions.

III. SIMULATION

This section describes two simulation results of dynamic 2D deformation of an inextensible linear object.

Figure 2 shows a sequence of deformed shapes of an inextensible linear object of length 1.00, bend rigidity 1.00, and line density 1.00 under gravity. The length is divided into 10 small intervals; implying that the deformation can be approximated by 11 nodal points. The left endpoint of the object is fixed to the coordinate origin but is free to rotate. Constant torque 5.00 is applied around the left endpoint. Runge-Kutta method with interval time 0.001 integrates a set of motion equations of the linear object. The initial shape at time 0.00 is plotted in Figure 2-(a). After 0.05 seconds, the left side of the object moves up because of the torque applied around the left endpoint while its right side moves down because of gravity, as plotted in Figure 2-(b). At time 0.15 through 0.30, curvature of the object takes larger values as before; suggesting that flexural potential energy is stored in the object, as shown in Figure 2-(d) through (g). At time 0.40, the right endpoint goes forward, as described in Figure 2-(i), after the stored potential energy is released. This simulation result given in the figures shows dynamic deformation of a linear object well qualitatively.

Figure 3 shows another sequence of deformed shapes of an inextensible linear object of length 1.00, bend rigidity 1.00, and line density 1.00 under gravity. The length is

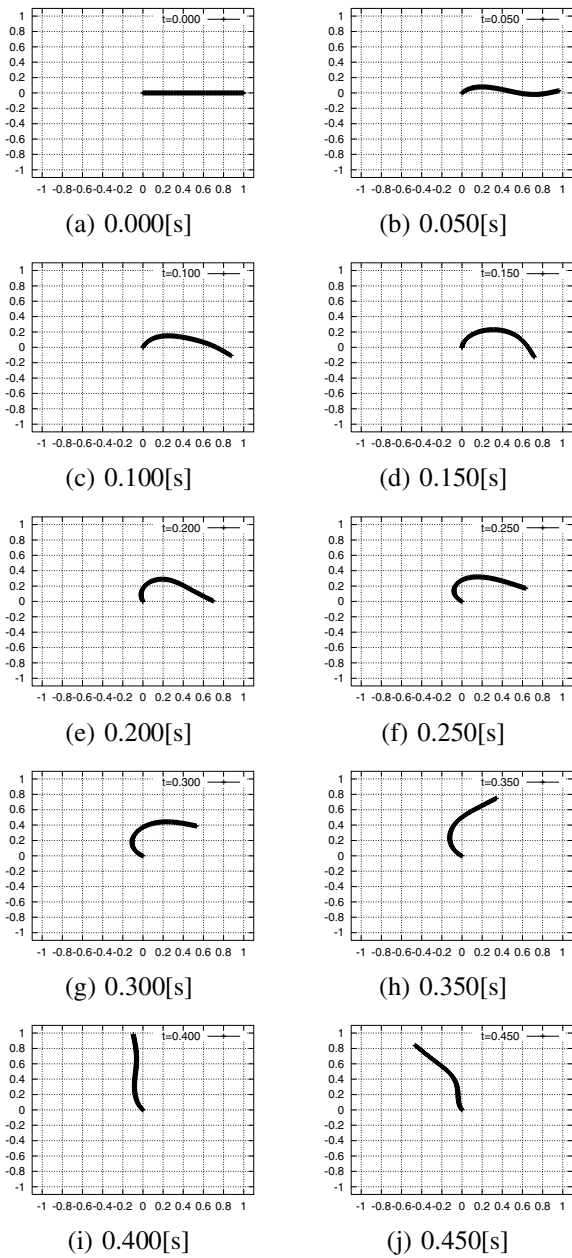


Fig. 2. Simulation of dynamic 2D deformation of linear object

divided into 10 small intervals; implying that the deformation can be approximated by 11 nodal points. The left endpoint is fixed to the coordinate origin and both ends are free to rotate. Runge-Kutta method with interval time 0.001 integrates a set of motion equations of the linear object. The distance between the two end points of the linear object is reduced to 0.6 along the horizontal line at its initial shape, as illustrated in Figure 3-(a). Namely, two positional constraints between the two endpoints are imposed on the object. After the two constraints are released at time 0.00, the right endpoint moves in the right direction, as plotted in Figure 3-(b) and (c), then it goes up as described in Figure 3-(d) and (e). After time 0.20, the left side falls

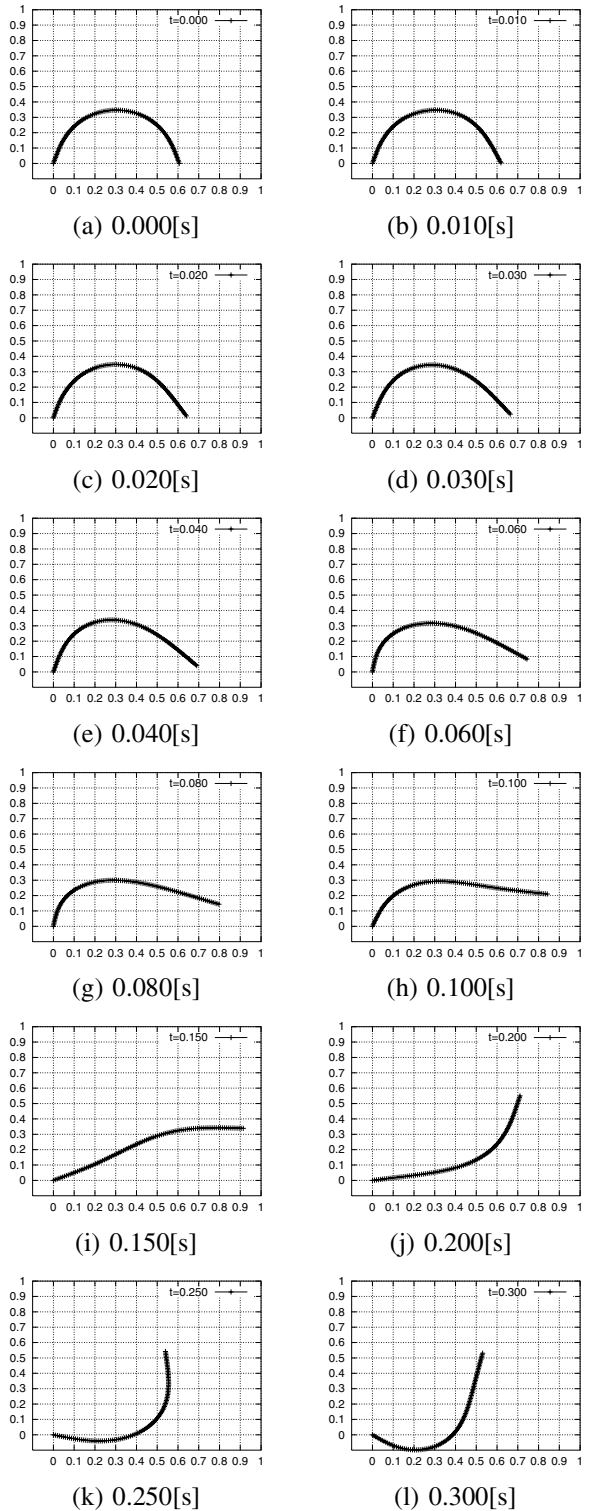


Fig. 3. Simulation of dynamic 2D deformation of linear object

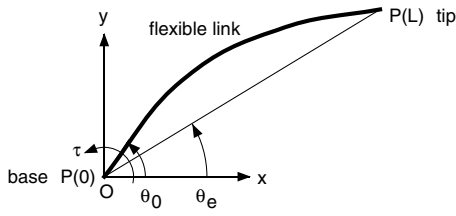


Fig. 4. Control of flexible link

down due to gravity, as described in Figure 3-(j) through (l). This simulation result given in the figures shows dynamic deformation of a linear object well qualitatively.

The above computations were performed on a 600MHz Alpha21164A CPU with 704MB memory operated by DIGITAL UNIX V4.0D. Programs were compiled by DEC C Compiler V5.6 with optimization option -O4. It took about 57 CPU seconds to compute one step of the dynamic deformation in both computations.

IV. CONTROL OF FLEXIBLE LINK

This section describes the control of a flexible link. Control of flexible manipulators has been extensively studied in the past decades. Many of the proposed control laws use strain signals to detect the deformation of a flexible manipulator[9], [10]. Strain signals are often noisy during the dynamic motion of a manipulator and tend to be blurred by an electromagnetic field due to actuators and their driving circuits. In this paper, we employ visual signals instead of strain signals to detect the deformation of a flexible structure.

We assume that the dynamic behavior of a flexible link can be described by 2D deformation of an inextensible linear object. Let θ_0 be the angle from the horizon at base point $P(0)$, where a torque is applied to a flexible link, as illustrated in Figure 4. Let θ_e denotes the angle from the horizon of vector connecting base point $P(0)$ and tip point $P(L)$. This angle is referred to as the *tip angle*. Note that the tip angle can be computed from the tip position observed by a vision system. Goal of a control law is to guide the tip angle θ_e to its desired angle θ_d and to suppress the vibration of the link. Let us first introduce the following PI term with respect to the tip angle so that the tip angle can be guided to its desired angle:

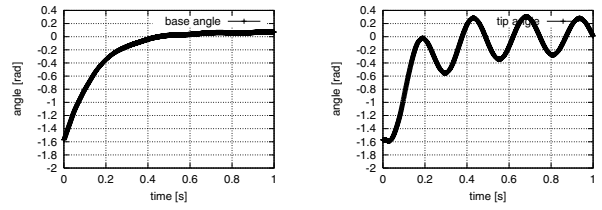
$$\tau_{\text{tip}} = K_p^e(\theta_d - \theta_e) + K_i^e \int_0^t (\theta_d - \theta_e) dt,$$

where K_p^e and K_i^e denote proportional and integral gains of tip angle feedback. Let us introduce the damping term given by

$$\tau_{\text{base}} = -K_d^0 \dot{\theta}_0,$$

where K_d^0 stands for a derivative gain of base angle feedback. Let us introduce the following term to suppress the vibration of the link:

$$\tau_{\text{sup}} = K_p^{\text{sup}}(\theta_e - \theta_0),$$

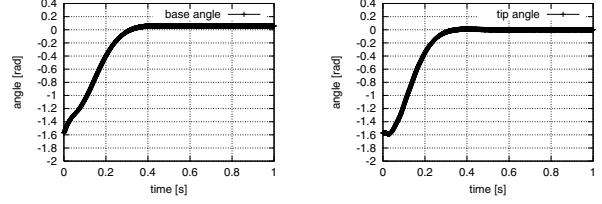


(a-1) base angle

(a-2) tip angle

(a) without vibration suppress term

$$(K_p^e = 1.0, K_i^e = 1.2, K_d^0 = 0.14, K_p^{\text{sup}} = 0.0)$$



(b-1) base angle

(b-2) tip angle

(b) with vibration suppress term

$$(K_p^e = 1.0, K_i^e = 1.2, K_d^0 = 0.14, K_p^{\text{sup}} = 3.5)$$

Fig. 5. Simulation results of control law

where K_p^{sup} represents a proportional gain. As a result, a control law for a flexible link is described as

$$\tau = \tau_{\text{tip}} + \tau_{\text{base}} + \tau_{\text{sup}}.$$

Simulation results are plotted in Figure 5. The desired angle θ_d is constantly equal to 0. Figure 5-(a) shows a result without vibration suppress term τ_{sup} . Figures 5-(a-1) and (a-2) describe the base and tip angles of a flexible link. As plotted in the figures, tip angle θ_e vibrates even after base angle θ_0 converges to a certain angle. Figure 5-(b) shows a result with the vibration suppress term. As plotted in Figures 5-(b-1) and (b-2), tip angle θ_e converges to its desired value as base angle θ_0 converges to a certain angle. Consequently, we find that the proposed vibration suppress term is effective to the control of a flexible link.

The proposed control law is experimentally verified. A flexible link composed of a spring steel of 0.5mm thickness is driven by an AC servo motor at the base point. An LED is attached to the tip point of the link. The position of the LED is detected using a 1000Hz vision system consisting of a CMOS image camera and an FPGA. A CMOS image camera ITL-HSC-AD-SDK can capture successive 1280×504 pixel images at 1000Hz. The captured images are sent to an FPGA, Xilinx Vertex-II 6000. Circuit to compute the image gravity center of a captured image is implemented on the FPGA to compute the position of the LED within 1msec. As a result, the vision system can detect the tip position of a flexible link at 1000Hz. The detected position is sent to a PC, which controls the flexible link according to the proposed control law.

Experimental results are plotted in Figure 6. The desired angle θ_d is constantly equal to 0. Figure 6-(a) shows a result without the vibration suppress term. As plotted in Figures 6-(a-1) and (a-2), tip angle θ_e vibrates even after base angle θ_0 converges to a certain angle. Figure 6-(b)

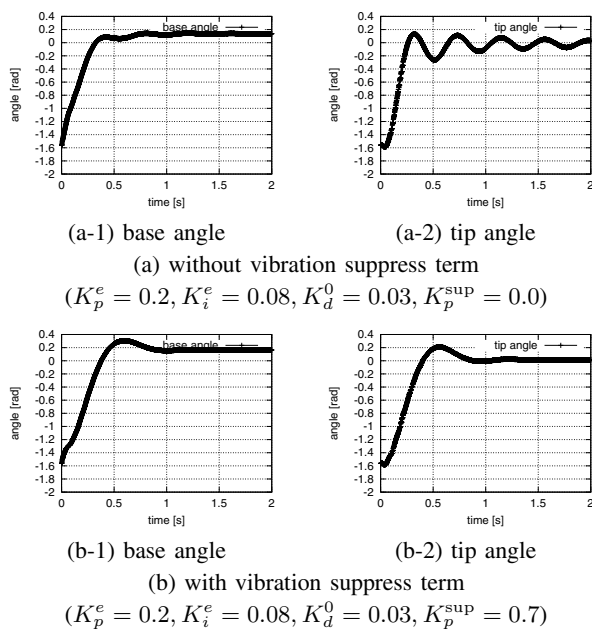


Fig. 6. Experimental results of control law

shows a result with the vibration suppress term. As plotted in Figures 6-(b-1) and (b-2), tip angle θ_e converges to its desired value as base angle θ_0 converges to a certain angle. Figures 7-(a) through (f) demonstrate the motion of the flexible link. From the above experiment, we find that the proposed vibration suppress term is effective to the control of a flexible link.

V. CONCLUDING REMARKS

We have described the dynamic modeling of linear object deformation based on differential geometry coordinates and its application to the control of a flexible link. First, we have formulated the 2D dynamic deformation of an inextensible linear object using differential geometry coordinates. A set of Lagrange equations of motion can be derived through finite element approximation of kinetic and potential energies of the object. Simulation results have demonstrated that the proposed method can compute the linear object deformation well. Next, we have applied the proposed dynamic modeling to the control of a flexible link. We have shown that a simple PI-control of the tip angle of a flexible link can guide the tip angle to its desired value without physical parameters of the link.

Future issues include 1) three-dimensional dynamic deformation and 2) application to knotting/unknotting of deformable linear objects. Differential geometry coordinates requires four independent functions to describe 3D deformation of a linear object. A set of Lagrange equations can be derived as well by applying finite element approximation to the four functions. Planning of knotting/unknotting of deformable linear objects requires physical simulation of the process. Dynamic simulation of linear object deformation can be applied to this simulation after formulating self-contact of a linear object in dynamics.

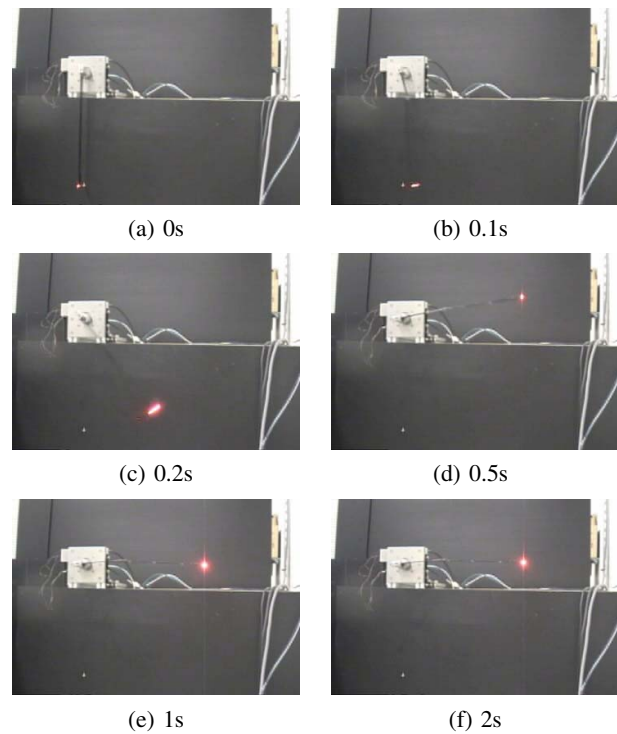


Fig. 7. Experimental result on vibration suppress control

ACKNOWLEDGEMENT

This research was supported in part by the Ritsumeikan University 21st Century COE program “Micro Nanoscience Integrated Systems”.

REFERENCES

- [1] Leaf, B. G. A. V., *Models of the Plain-Knitted Loop*, Journal of the Textile Institute Transactions, pp.49–58, 1960.
- [2] Rosenblum, R. E., Carlson, W. E., and Tripp, E., *Simulating the Structure and Dynamics of Human Hair: Modelling, Rendering and Animation*, Journal of Visualization and Computer Animation, 2(4):141–148, 1991.
- [3] Daldegan, A., Thalmann, N. M., Kurihara, T., and Thalmann, D., *An Integrated System for Modeling, Animating and Rendering Hair*, Computer Graphics Forum (Eurographics '93), 12(3):211–221, 1993.
- [4] Kühnapfel, U., Çakmak, H. K., and Maass, H., *Endoscopic surgery training using virtual reality and deformable tissue simulation*, Computers & Graphics, Vol. 24, No. 5, pp.671–682, 2000.
- [5] Timoshenko, S., *Strength of Materials Part I Elementary Theory and Problems*, D. Van Nostrand Company, Inc., 1955.
- [6] Belytschko, T., Liu, W. K., and Moran, B. *Nonlinear Finite Elements for Continua and Structures*, John Wiley & Sons, Chapter 9 Beams and Shells, pp.509–568, 2000.
- [7] Pai, D. K., *STRANDS: Interactive Simulation of Thin Solids using Cosserat Models*, Computer Graphics Forum. 21(3), pp.347–352, 2002.
- [8] Wakamatsu, H. and Hirai, S., *Static Modeling of Linear Object Deformation Based on Differential Geometry*, International Journal of Robotics Research, Vol.23, No.3, March, pp.293–311, 2004.
- [9] Ge, S. S., Lee, T. H., and Zhu, G., *Improving Joint PD Control of Single-link Flexible Robots by Strain/Tip Feedback*, Proc. of IEEE International Conference on Control Applications, Dearborn, pp.965–969, 1996.
- [10] Matsuno, F., Ohno, T., and Orlov, Y. V., *Proportional Derivative and Strain (PDS) Boundary Feedback Control of a Flexible Space Structure with a Closed-Loop Chain Mechanism*, Automatica, 38(7), pp.1201–1211, 2002.